

Stress percolation criticality of glass to fluid transition in active cell layers

Siavash Monfared,^{1,2,*} Guruswami Ravichandran,¹ José E. Andrade,¹ and Amin Doostmohammadi^{2,†}

¹*Division of Engineering and Applied Science, California Institute of Technology, Pasadena, CA 91125, USA.*

²*Niels Bohr Institute, University of Copenhagen, Denmark.*

(Dated: October 18, 2022)

Using three-dimensional representation of confluent cell layers, we map the amorphous solid to fluid phase transition in active cell layers onto the two-dimensional (2D) site percolation universality class. Importantly, we unify two distinct, predominant, pathways associated with this transition; namely (i) cell-cell adhesion and (ii) active traction forces. For each pathway, we independently vary the corresponding control parameter and focus on the emergent mechanical stress patterns as the monolayer transitions from a glassy- to a fluid-like state. Through finite-size scaling analyses, our results lead us to establish the glassy- to fluid-like transition as a critical phenomena in terms of stress development in the cell layer and show that the associated criticality belongs to the 2D site percolation universality class. Our findings offer a fresh perspective on solid (glass-like) to fluid phase transition in active cell layers and can bridge our understanding of glassy behaviors in active matter with potential implications in biological processes such as wound healing, development, and cancer progression.

The transition between solid (glass-like) and fluid phases in cellular systems is of fundamental relevance to a range of biological processes, including cancer metastasis [1–3], wound healing [4–6] and tissue morphogenesis [7–9]. Over the past decade, this transition is revealed to be governed by collective cell organization in biological tissues [10–14], spurring a plethora of research on this topic [9, 15–17]. To understand the solid-fluid transition in biological systems, the concept of jamming has been applied to inherently out-of-equilibrium living cells [18–20] where jamming-unjamming is used to refer to the transition between solid-like glassy and fluid-like states. This is despite the geometrical roots of jamming transition and its correspondence to the zero temperature and zero activity limit of a glass transition [21–24]. In this vein, non-equilibrium glass transition in active systems share many features with equilibrium glass transition [25] and an effective thermodynamic equilibrium may prevail for moderate activity driving the system out-of-equilibrium [26].

Over the past decade, the glass-like to fluid transition in living cells is broadly understood as a geometric jamming transition characterized by a critical shape index $q = \mathcal{P}/\sqrt{\mathcal{A}}$, where \mathcal{P} and \mathcal{A} are cell perimeter and area respectively. This is primarily based on the application of two-dimensional vertex models [19, 27], a voronoi based variant endowed with motility [28] and experiments on a range of epithelial systems [20] underlining the role of geometrical constraints. More recent studies highlight the role of two types of percolations based on (i) cell connectivity [29] and (ii) edge tension network [30, 31]. In particular, experiments on a zebrafish blastoderm [8], a non-confluent cell system with synchronous cell divisions, show a solid-fluid transition at the onset of zebrafish morphogenesis. This transition is linked to a rigidity percolation based on cell connectivity [29]. On the other hand, application of a vertex model to het-

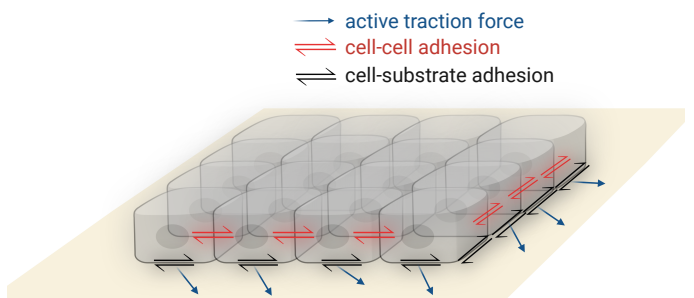


FIG. 1. Schematic of a confluent layer displaying cell-cell and cell-substrate adhesions and in-plane active traction forces acting on the plane of the substrate (illustrated as yellow surface). Created with BioRender.com

erogeneous cell layers [30] and experiments on primary tumour explants [31] show rigidity percolation based on edge tension network gives rise to finite shear modulus in tumor explants consisting of heterogeneous mixture of soft and stiff cancer cells. Notwithstanding these seminal and important contributions, the universality of the transition between active solid (glass-like) and fluid phases in cellular systems and its broader applicability is yet to be established [7, 29, 32–37]. Therefore, despite the immense significance of transition from glassy- to fluid-like state in cell collectives in various biological processes, the nature of transition remains elusive.

Here, we characterize the criticality of the active glass-to-fluid transition in cell layers. Importantly, we establish this through two distinct paths by varying, independently, cell-cell adhesion and active traction forces as control parameters and recover the 2D site percolation critical exponents for isotropic stress clusters via finite-size scaling analyses.

We build on a recently developed three-dimensional phase-field model for cell layers, which allows for inde-

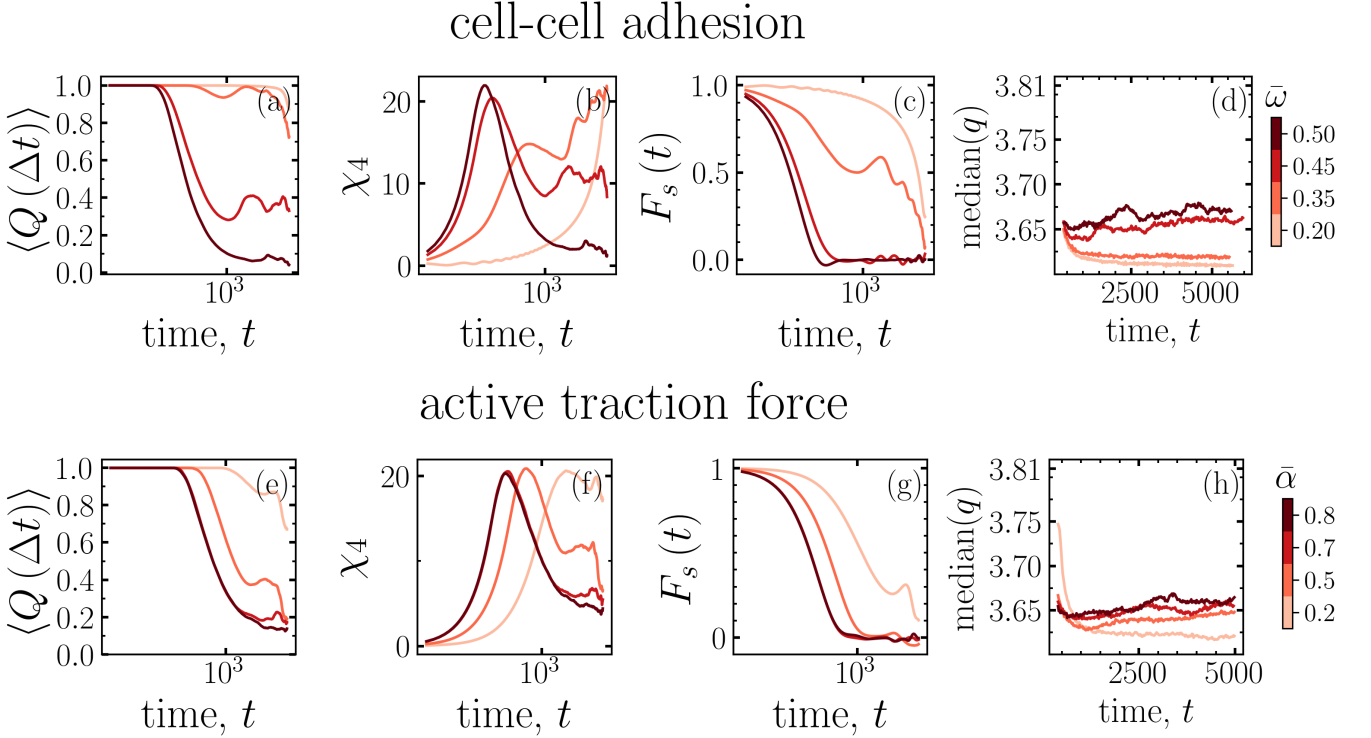


FIG. 2. Quantitative characterization of cell mobility in terms of overlap function (a,e), four-point susceptibility (b,f) and self-scattering function (c,g) as cell-cell adhesion (a,b,c) and active traction force strength (e,f,g) are increased. The temporal evolution of the median of shape parameter, q with increasing $\bar{\omega}$ (d) and $\bar{\alpha}$ (h).

pendent variation of cell-cell and cell-substrate interactions [38]. We consider a cellular monolayer consisting of $N = 400$ cells on a substrate with its surface normal $\vec{e}_n (= \vec{e}_z) = \vec{e}_x \times \vec{e}_y$ and periodic boundaries in both \vec{e}_x and \vec{e}_y , where $(\vec{e}_x, \vec{e}_y, \vec{e}_z)$ constitute the global orthonormal basis (see Fig. 1). Each cell i is modeled as an active deformable droplet in three-dimensions using a phase-field, $\phi_i = \phi_i(\vec{x})$ and initialized with radius R_0 . The interior and exterior of cell i corresponds to $\phi_i = 1$ and $\phi_i = 0$, respectively, with a diffuse interface of length λ connecting the two regions and the midpoint, $\phi_i = 0.5$, delineating the cell boundary.

This approach resolves the cellular interfaces and provides access to intercellular forces. The dynamics of the phase field ϕ_i is evolved through:

$$\partial_t \phi_i + \vec{v}_i \cdot \vec{\nabla} \phi_i = -\frac{\delta \mathcal{F}}{\delta \phi_i}, \quad i = 1, \dots, N, \quad (1)$$

where \vec{v}_i is the velocity of cell i and $\mathcal{F}[\phi]$ is the three-dimensional free energy functional that stabilizes cell interface and accounts for cell mechanical properties including cell stiffness (E) and compressibility (μ), and puts a soft constraint on the cell volume [39–42] around $V_0 = (4/3)\pi R_0^3$. Additionally, the free energy comprises gradient contributions ($\vec{\nabla}\phi$) that account for, and distinguish between, cell-cell (ω_{cc}) and cell-substrate (ω_{cw})

adhesions, as introduced recently [38]:

$$\begin{aligned} \mathcal{F} = & \sum_i^N \frac{E}{\lambda^2} \int d\vec{x} \{ 4\phi_i^2 (1 - \phi_i)^2 + \lambda^2 (\vec{\nabla} \phi_i)^2 \} \\ & + \sum_i^N \mu \left(1 - \frac{1}{V_0} \int d\vec{x} \phi_i^2 \right)^2 + \sum_i^N \sum_{j \neq i} \frac{\kappa_{cc}}{\lambda} \int d\vec{x} \phi_i^2 \phi_j^2 \\ & + \sum_i^N \sum_{j \neq i} \frac{\omega_{cc}}{\lambda^2} \int d\vec{x} \vec{\nabla} \phi_i \cdot \vec{\nabla} \phi_j + \sum_i^N \frac{\kappa_{cw}}{\lambda} \int d\vec{x} \phi_i^2 \phi_w^2 \\ & + \sum_i^N \frac{\omega_{cw}}{\lambda^2} \int d\vec{x} \vec{\nabla} \phi_i \cdot \vec{\nabla} \phi_w, \end{aligned} \quad (2)$$

where κ captures repulsion between cell-cell (subscript cc) and cell-substrate (subscript cw) and ϕ_w denotes a static phase-field representing the substrate. To resolve the forces generated at the cellular interfaces, we consider the following over-damped dynamics for cells:

$$\vec{T}_i = \zeta \vec{v}_i - \vec{F}_i^{\text{act}} = \int d\vec{x} \phi_i \vec{\nabla} \cdot \left(\sum_i -(\delta \mathcal{F}/\delta \phi_i) \right) \mathbf{1} \quad (3)$$

where \vec{T}_i denotes traction [11, 43, 44] and contains both active and passive contributions, ζ is substrate friction and $\vec{F}_i^{\text{act}} = \alpha \hat{F}_i^{\text{pol}}$ represents self-propulsion force directed by cell polarity, constantly pushing the system

out-of-equilibrium with α characterizing the strength of the self-propulsion force, and \hat{F}_i^{pol} a unit vector corresponding to the polarity direction for each cell. The dynamics of cell polarity is introduced based on contact inhibition of locomotion [45, 46] by aligning the polarity of the cell to the direction of the total interaction force acting on the cell [47], and is chosen specifically based on recent experimental observations [48] (see *Materials and Methods*). Throughout this study we use the initial cell radius R_0 as the characteristic length scale, the polarity alignment time τ as the characteristic time scale, and the cell stiffness E as the characteristic force scale to report the results in dimensionless units (see *Materials and Methods*).

In passive, athermal systems, jamming transition is intimately related to the packing fraction (density) of that system. However, for living cells at confluence, the collective behavior can change from a fluid-like to a solid (glass-like) behavior at a constant density. In recent studies, density is also shown to have a second order effect on fluid-solid transition in cellular systems [18]. With this in mind, we keep the cell density constant in our simulations, i.e. we do not allow cell proliferation nor cell extrusion, while ensuring confluency. For each considered pathway, we perform large scale simulations by incrementally increasing the dimensionless cell-cell to cell-substrate adhesion ratio $\bar{\omega} = \omega_{cc}/\omega_{cw} \in [0.1, 0.5]$ for the first, and the dimensionless traction force $\bar{\alpha} = \alpha\tau/\zeta R_0$, $\bar{\alpha} \in [0, 0.8]$, which characterizes the ratio of self-propulsion to the friction with the substrate, for the second pathway. For each case, three distinct realizations and $n_{\text{sim}} = 5000$ time steps are considered. As we show next, the considered ranges for $\bar{\omega}$ and $\bar{\alpha}$ captures the glassy- to fluid-like state of cells. Other simulation parameters are fixed and outlined in the *Materials and Methods*.

We begin by establishing what constitutes as a glassy state, which is necessary to identify the onset of glassy- to fluid-like phase transition. To this end, we characterize cell displacement and cooperative cell motion as a function of the two control parameters, i.e. dimensionless cell-cell adhesion $\bar{\omega}$, and strength of traction force $\bar{\alpha}$ (Fig. 2).

First we quantify the overlap function, the fractional change of cellular position in a given time increment Δt , $Q(\Delta t) = (1/N) \sum_{i=1}^N w_i$, where $w = 1$ if $|\vec{x}_i(t + \Delta t) - \vec{x}_i(t)| < R_0$ and $w = 0$, otherwise. As the strength of cell-cell adhesion $\bar{\omega}$, and the self-propulsion force $\bar{\alpha}$ increase, the overlap function falls below 0.2, reflecting the high mobility of the cells and potentially exchanging neighbors in a fluid-like state (Fig. 2a,e).

To quantify the cooperative motions of cells, we use the overlap function, $Q(\Delta t)$, to compute the four-point susceptibility, $\chi_4 = N[\langle Q(\Delta t)^2 \rangle - \langle Q(\Delta t) \rangle^2]$. When cells move cooperatively, χ_4 exhibits a clear peak with its position and magnitude corresponding to pack lifetime

and pack size, approximately [49]. For a solid (glass-like) state, typically the swirl lifetime grows and exceeds the temporal window of observation, in our case that is the total simulation time. For both the strong cell-cell adhesion, $\bar{\omega} = 0.5$, and self-propulsion force strength $\bar{\alpha} = 0.8$, a fluid-like state is observed. This is evident from the overlap function $\langle Q(\Delta t) \rangle$ indicating the formation of a pack of ~ 20 cells with a lifetime of ~ 400 time steps, in dimensionless units (Fig. 2b,f). For the adhesion or self-propulsion strengths lower than this critical value, peaks in χ_4 are observed, with the pack size increasing as the adhesion or self-propulsion force strength is increased.

To complete the characterization of the glassy dynamics we also quantify the self-scattering function, $F_s(k, t) = \langle e^{i\vec{k} \cdot \Delta\vec{r}(t)} \rangle$ where $|\vec{k}| = \pi/r_0$, and r_0 is the position of the first peak in the pair-correlation function. Consistent with the characterization of the overlap function and four-point susceptibility, for the highest value of cell-cell adhesion, F_s approaches zero indicative of a fluid-like state (Fig. 2c). For $\bar{\omega} \ll 0.5$, F_s is around one suggesting a glass state. Similar behavior is observed for the strength of self-propulsion force $\bar{\alpha} \ll 0.8$ (Fig. 2g). Together, the results of the measurements of the overlap function, four-point susceptibility, and the self-scattering function confirm that upon increasing the ratio of cell-cell adhesion to cell-substrate adhesion, or independently, increasing the self-propulsion force, the active cell layer continuously transitions from a solid (glassy) state to a fluid-like state. Particularly, based on the presented analyses of cell cooperative motions, this transition takes place at $\bar{\omega} = 0.5$ and $\bar{\alpha} = 0.8$.

The results discussed so far, indicating a glass-to-fluid transition upon increasing cell-cell adhesion or self-propulsion force, is consistent with the previous results observed in experiments and vertex models of cell layers [18, 20, 28]. To this end, our point of departure from the previous characterization of the active glass-to-fluid transition in cell layers is that by accounting for both cell-cell and cell-substrate interactions we do not observe any geometric signatures for jamming transition associated with the shape order parameter. This is evident from Fig. 2d,h where we compute the projected area and the perimeter for each cell and every simulation time steps and compute the cell shape index, q . At all times after the initialization, for both glassy- and fluid-like systems, the median for the shape index, \bar{q} remains under $\bar{q} = 3.75$, clearly deviating from the value of $\bar{q} \approx 3.81$ that has been suggested as the structural order parameter for solid-to-fluid jamming transition in cell layers [19]. Similar deviation has been observed in experiments on zebrafish embryo and the associated active vertex model that allows for finite extracellular spaces between the cells [36]. Moreover, detailed analysis of the voronoi based model [28] has find no geometric jamming transition at the zero temperature limit [32]. Additionally, recent experiments on Madin-Darby canine kidney

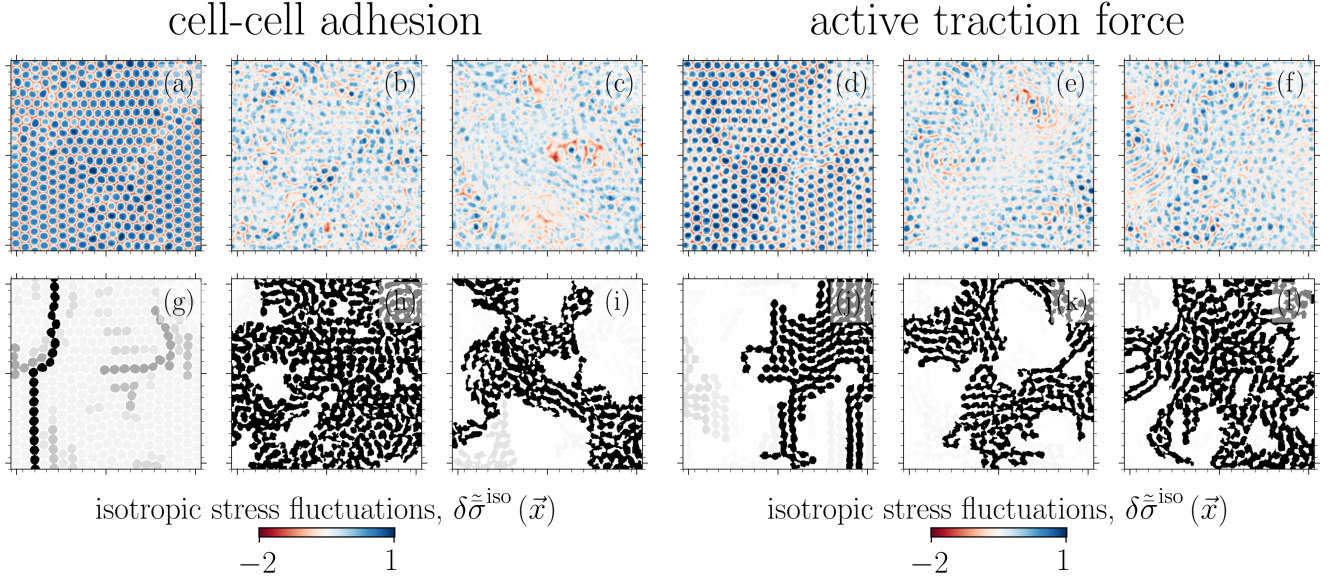


FIG. 3. Percolation of isotropic stress within the cell layer. The fluctuations in normalized temporal average of the isotropic stress field, $\delta\tilde{\sigma}^{\text{iso}} = \tilde{\sigma}^{\text{iso}} - \langle \tilde{\sigma}^{\text{iso}} \rangle$, $\tilde{\sigma}^{\text{iso}}(\vec{x}) = \bar{\sigma}^{\text{iso}} / \sigma_{\max}^{\text{iso}}$ where $\sigma^{\text{iso}} = (1/3)\text{tr}\boldsymbol{\sigma}$ for increasing dimensionless cell-cell adhesion (a) $\bar{\omega} = 0.2$, (b) $\bar{\omega} = 0.45$ and (c) $\bar{\omega} = 0.5$. The largest spanning cluster (in Black) corresponding to $\tilde{\sigma}^{\text{iso}}(\vec{x})$ for (g) $\bar{\omega} = 0.2$ percolating at $\rho = 0.743$, (h) $\bar{\omega} = 0.45$ percolating at $\rho = 0.647$, and (i) $\bar{\omega} = 0.5$ percolating at $\rho = 0.525$ and dimensionless active traction strength $\bar{\alpha}$ for (d) $\bar{\alpha} = 0.2$, (e) $\bar{\alpha} = 0.7$ and (f) $\bar{\alpha} = 0.8$. The largest spanning cluster (in Black) corresponding to $\tilde{\sigma}^{\text{iso}}(\vec{x})$ for (j) $\bar{\alpha} = 0.2$ percolating at $\rho = 0.622$, (k) $\bar{\alpha} = 0.7$ percolating at $\rho = 0.540$, and (l) $\bar{\alpha} = 0.8$ percolating at $\rho = 0.599$.

(MDCK) cells do not show such geometric criticality and through various molecular perturbations establish that the change in adhesion strength has no effect on the cell perimeter, instead demonstrating that the traction forces play a dominant role in glass to fluid phase transition in the epithelial tissues [35].

Rather than geometric considerations, to understand the glass transition in the considered confluent active cell layers, we turn to the emergent mechanical stress fields. To this end, we compute a coarse-grained stress field [50]:

$$\sigma_{ij} = \frac{1}{2V_{cg}} \sum_{m \in V_{cg}} \left(\vec{T}_i(\vec{x}_m) \otimes \vec{e}_j^n + \vec{T}_j(\vec{x}_m) \otimes \vec{e}_i^n \right) \quad (4)$$

where \vec{x}_0 represents the center of the coarse-grained volume, $V_{cg} = \ell_{cg}^3$, corresponding to coarse-grained length $\ell_{cg} = a_0$ where a_0 is the unit grid length, and unit vector $\vec{e}_i^n = (\vec{x}_0 - \vec{x}_m) / |\vec{x}_0 - \vec{x}_m|$. Given the definition of \vec{T}_i in (3), the coarse grained stress field, (4), contains contributions from both active and passive forces. To probe for a possible mechanical criticality at the active glass-to-fluid transition, we then measure the temporally averaged isotropic stress field $\tilde{\sigma}^{\text{iso}}(\vec{x}) = \bar{\sigma}^{\text{iso}}(\vec{x}) / \bar{\sigma}_{\max}^{\text{iso}}(\vec{x})$, where $\bar{\sigma}^{\text{iso}}(\vec{x}) = (1/n_{\text{sim}}) \sum_t^{n_{\text{sim}}} \sigma^{\text{iso}}(\vec{x}, t)$, with n_{sim} number of simulation time steps and $\sigma^{\text{iso}}(\vec{x}, t) = (1/3) \text{tr} \boldsymbol{\sigma}(\vec{x}, t)$, provides a measure of the amount of expansion ($\sigma^{\text{iso}} > 0$) and compression ($\sigma^{\text{iso}} < 0$) in the cell layer. Visual inspection of the fluctuations in isotropic stress fields and the associated patterns shows that for both adhesion parameter $\bar{\omega}$ (Figs. 3a-c) and traction force $\bar{\alpha}$ (Figs. 3d-f),

as the control parameter is increased and the system approaches a fluid-like state, a more disordered isotropic stress field emerges, suggesting a possible percolation of isotropic stress in the system. Figs. 3g-l display the spanning cluster - a cluster of connected sites that spans two opposing sides of the system's boundary - in Black, for each pathway as $\bar{\omega}$ or $\bar{\alpha}$ is increased. To quantify this emergent build up and the possible links to percolation universality classes, we perform a finite-size scaling analysis [51, 52] for each path. We begin with quantifying the density of the spanning cluster, $P(p, L)$, which is the probability of a site belonging to a spanning cluster as a function of the occupation probability, p , and system size, L . The occupation probability, $p \in [0, 1]$, corresponds to sites where $\tilde{\sigma}^{\text{iso}}(\vec{x})$ is greater than $(1-p) \times 100$ -th percentile of the isotropic stress distribution. In the thermodynamic limit, i.e. $L \rightarrow \infty$, we expect the following power-law scaling near the percolation probability, p_c for the density of spanning cluster $P(p)$ characterized by critical exponent β :

$$P(p) \sim (p - p_c)^\beta. \quad (5)$$

Furthermore, we quantify the average cluster size, $S(p) = \langle s \rangle$ where s is size of a cluster. Near the percolation probability, the power-law scaling of $S(p)$ quantified by critical exponent γ reads:

$$S(p) \sim |p - p_c|^{-\gamma}, \quad (6)$$

and critical exponent ν which describes the power-law

cell-cell adhesion

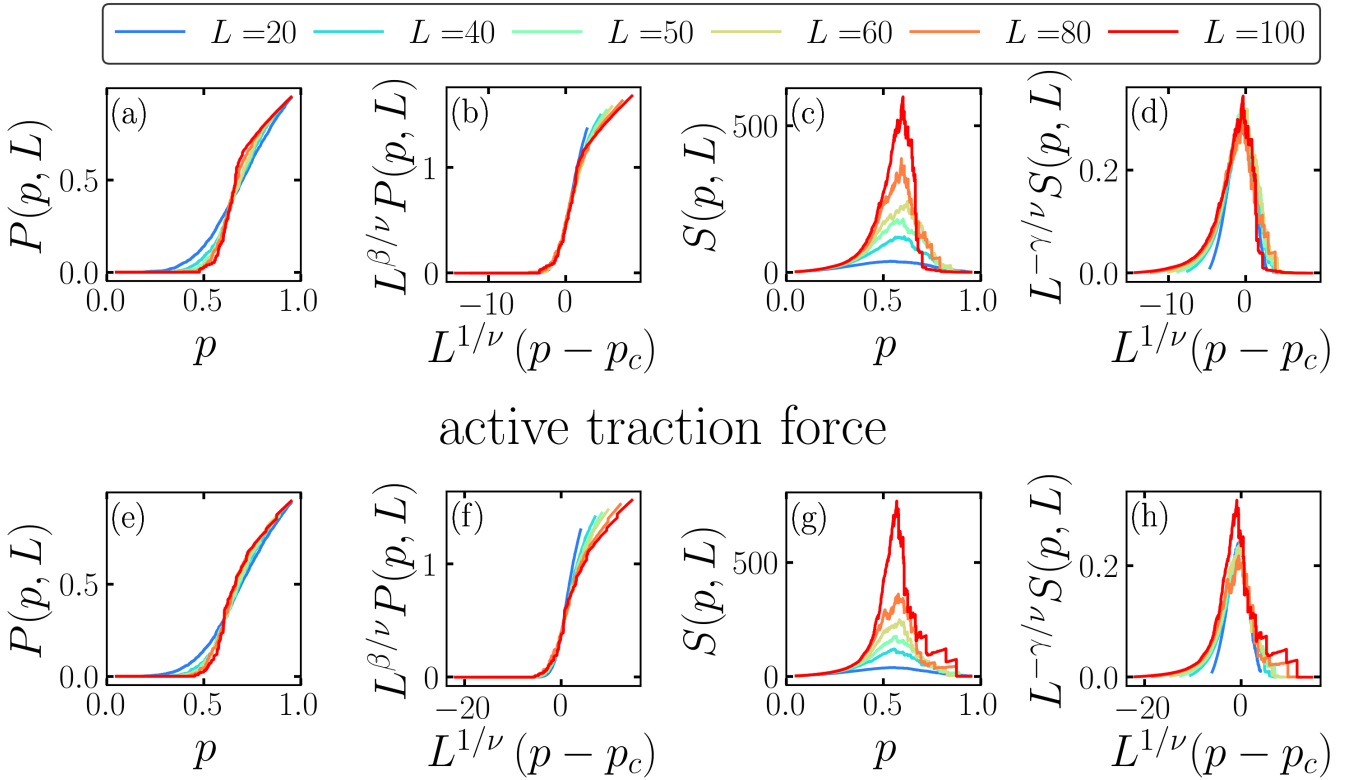


FIG. 4. Finite-size scaling analyses of isotropic stress criticality. The density of spanning cluster $P(p, L)$ (a,e) and the average cluster size $S(p, L)$ at different length scales L and their collapse after performing a finite size scaling analysis for $P(p, L)$ (b,f) and $S(p, L)$ (c,h). First row (a-d) corresponds to increasing dimensionless cell-cell adhesion $\bar{\omega} = \omega_{cc}/\omega_{cw}$ and the second row (e-h) corresponds to increasing strength of active traction forces $\bar{\alpha}$.

scaling of correlation length ξ , an average distance between two sites in the same cluster, is expected to follow:

$$\xi \sim |p - p_c|^{-\nu}. \quad (7)$$

Both the density of the spanning cluster, $P(p, L)$ and the average cluster size $S(p, L)$ are displayed in Fig. 4 at the onset of the transition, i.e. $\bar{\omega} = 0.45 < 0.5$ (Fig. 4a,c) and $\bar{\alpha} = 0.7 < 0.8$ (Fig. 4e,g) for various length scales, L . Additionally, Fig. 4b,d,f,h show the collapse of $P(p, L)$ and $S(p, L)$ when scaled with critical exponents obtained from the finite-size scaling analysis, accounting for a diverging correlation length ξ near the p_c , i.e. (7). Remarkably, the critical exponents corresponding to the scaling of temporally averaged isotropic stress field at the onset of the glass-to-fluid transition in the active cell layer (Tab. I) lead to a reasonable collapse and are in close agreement with those from the 2D site-percolation universality class [53] (see supporting information for more details regarding finite-size scaling analysis). Importantly, the agreement with the critical exponents for 2D site-percolation universality class are obtained for two independent pathways (i.e., cell-cell ad-

hesion and active traction force) of driving the system through glass-to-fluid transition, further reinforcing the universality of the isotropic stress percolation at the onset of active glass-to-fluid transition in model cell layers. Moreover, a recent study suggest that the microscopic details of self-propulsion does not affect the glassy dynamics of active systems [54]. This implies that our presented analyses would hold irrespective of how we introduce active self-propulsion forces, $\vec{F}_i^{\text{act}} = \alpha \hat{F}_i^{\text{pol}}$ (see *Materials and Methods* for details regarding the dynamics of cell polarity).

Our findings contribute to the mounting evidence that suggest the existence of critical phenomena and universality classes in diverse range of active and biological systems including a first-order phase transition associated with the cell plasticity [55, 56], *epithelial-to-mesenchymal* (EMT) during tissue spreading as a wetting transition [57, 58], and viscosity changes due to rigidity percolation in fly embryo [29].

Our results can also help guide the conversation on the origins of density-independent solid-to-fluid phase transition in biological systems. Currently, the consensus on

TABLE I. Critical exponents obtained from finite size scaling analysis.

	p_c	γ	β	ν
2D site percolation [53]	0.5927	2.388	0.1388	1.333
This study ($\bar{\omega}$)	0.612 ± 0.004	2.305 ± 0.146	0.176 ± 0.049	1.422 ± 0.051
This study ($\bar{\alpha}$)	0.590 ± 0.007	2.103 ± 0.423	0.134 ± 0.009	1.243 ± 0.198

dominant mechanisms responsible for such a transition are: (i) shape order parameter, (ii) rigidity percolation based on cell-cell connectivity modulated by cell-cell adhesion and (iii) percolation of mechanical tension. All of these mechanisms are implicitly manifested in stress fields and thus our findings, including the mapping to the 2D site percolation universality class, can potentially unify previously reported experimental and theoretical observations. To this end, our work opens new possibilities to further investigate the nature of glass-to-fluid transition in active systems using the tools of non-equilibrium statistical mechanics and to explain transitionary behaviours in biological systems. Moreover, the reported findings call for development of new theoretical formulations to explain active glass-to-fluid transition based on emerging stress patterns and the criticality of the isotropic stress percolation. Simultaneously, direct measurement of traction forces and mechanical stress fields produced by multicellular layers is currently experimentally accessible [43, 59] and can be used to probe the proposed universality in cellular monolayers in experiments.

Lastly, it would be interesting to further study any possible connections between these results and those for glass transition and jamming in passive, weakly connected amorphous solids and granular materials. Particularly intriguing is the association of jamming in passive systems with the emergence of rigidity [60, 61] and a variety of percolation models [62–64].

Simulation parameters

We consider a cellular monolayer consisting of $N = 400$ cells on a substrate with its surface normal $\vec{e}_n (= \vec{e}_z) = \vec{e}_x \times \vec{e}_y$ and periodic boundaries in both \vec{e}_x and \vec{e}_y , where $(\vec{e}_x, \vec{e}_y, \vec{e}_z)$ constitute the global orthonormal basis. Cells are initiated on a two-dimensional simple cubic lattice and inside a cuboid of size $L_x = L_y = 320$, $L_z = 64$, grid size $a_0 = 1$ and with radius $R_0 = 8$. Simulations are run for $n_{\text{sim}} = 5000$ time steps. We perform large scale simulations with a focus on the interplay of cell-cell and cell-substrate adhesion strengths on collective cell migration and its impact on cell expulsion from the monolayer. Following [42], the space and time discretization in our simulations are based on the average radius of MDCK cells, $\sim 5\mu\text{m}$, velocity $\sim 20\mu\text{m}/\text{h}$ and average pressure of $\sim 100\text{Pa}$, measured experimentally in MDCK mono-

layers [44], corresponding to $\Delta x \sim 0.5\mu\text{m}$, $\Delta t \sim 0.1\text{s}$ and $\Delta F \sim 1.5\text{nN}$ for force. The simulation parameters $\kappa_{\text{cc}} = 0.5$, $\kappa_{\text{cw}} = 0.15$, $\zeta = 1$, $E = 0.024$, $\mu = 45$, $D_r = 0.01$ and $\tau = 200$, are chosen in the range that was previously shown successful for comparison of phase-field model with experimental measurements of sustained oscillations [48] and characterization of flows and topological defects in epithelial cell monolayer. For the first path to transition with cell-cell adhesion as the control parameter, $\bar{\alpha} = 1.25$ and for the second path with active traction force as the control parameter, $\bar{\omega} = 0.5$.

Dynamics of cell polarity

The dynamics of cell polarity is introduced based on contact inhibition of locomotion [45, 46] by aligning the polarity of the cell to the direction of the total interaction force acting on the cell [47, 48]. As such, the polarization dynamics is given by:

$$\partial_t \theta_i = -\frac{1}{\tau} |\vec{T}_i| \Delta \theta_i + D_r \eta, \quad (8)$$

where $\theta_i \in [-\pi, \pi]$ is the counterclockwise angle of cell polarity measured from \vec{e}_x , $\hat{F}_i^{\text{pol}} = (\cos \theta_i, \sin \theta_i)$ and η is the Gaussian white noise with zero mean, unit variance, D_r is rotational diffusivity, $\Delta \theta_i$ is the angle between \hat{F}_i^{pol} and \vec{T}_i , and positive constant τ sets the alignment time scale.

Acknowledgments

S.M. is grateful for the generous support of the Rosenfeld Foundation fellowship at the Niels Bohr Institute, University of Copenhagen. S.M., G.R. and J.A. acknowledge support for this research provided by US ARO funding through the Multidisciplinary University Research Initiative (MURI) Grant No. W911NF-19-1-0245. A. D. acknowledges funding from the Novo Nordisk Foundation (grant No. NNF18SA0035142 and NERD grant No. NNF21OC0068687), Villum Fonden Grant no. 29476, and the European Union via the ERC-Starting Grant PhysCoMeT.

* siavash.monfared@nbi.ku.edu

[†] doostmohammadi@nbi.ku.dk

- [1] L. Oswald, S. Grosser, D. M. Smith, and J. A. Käs, Jamming transitions in cancer, *Journal of physics D: Applied physics* **50**, 483001 (2017).
- [2] S. Grosser, J. Lippoldt, L. Oswald, M. Merkel, D. M. Sussman, F. Renner, P. Gottheil, E. W. Morawetz, T. Fuhs, X. Xie, S. Pawlizak, A. W. Fritsch, B. Wolf, L.-C. Horn, S. Briest, B. Aktas, M. L. Manning, and J. A. Käs, Cell and nucleus shape as an indicator of tissue fluidity in carcinoma, *Physical Review X* **11**, 10.1103/physrevx.11.011033 (2021).
- [3] E. Blauth, H. Kubitschke, P. Gottheil, S. Grosser, and J. A. Käs, Jamming in embryogenesis and cancer progression, *Frontiers in Physics* **9**, 10.3389/fphy.2021.666709 (2021).
- [4] J. H. Kim, X. Serra-Picamal, D. T. Tambe, E. H. Zhou, C. Y. Park, M. Sadati, J.-A. Park, R. Krishnan, B. Gweon, E. Millet, J. P. Butler, X. Trepaut, and J. J. Fredberg, Propulsion and navigation within the advancing monolayer sheet, *Nature Materials* **12**, 856 (2013).
- [5] R. J. Tetley, M. F. Staddon, D. Heller, A. Hoppe, S. Banerjee, and Y. Mao, Tissue fluidity promotes epithelial wound healing, *Nature Physics* **15**, 1195 (2019).
- [6] A. Jain, V. Ulman, A. Mukherjee, M. Prakash, M. B. Cuencia, L. G. Pimpale, S. Münster, R. Haase, K. A. Panfilio, F. Jug, S. W. Grill, P. Tomancak, and A. Pavlopoulos, Regionalized tissue fluidization is required for epithelial gap closure during insect gastrulation, *Nature Communications* **11**, 10.1038/s41467-020-19356-x (2020).
- [7] A. Mongera, P. Rowghanian, H. J. Gustafson, E. Shelton, D. A. Kealhofer, E. K. Carn, F. Serwane, A. A. Lucio, J. Giannona, and O. Campàs, A fluid-to-solid jamming transition underlies vertebrate body axis elongation, *Nature* **561**, 401 (2018).
- [8] N. I. Petridou, S. Grigolon, G. Salbreux, E. Hannezo, and C.-P. Heisenberg, Fluidization-mediated tissue spreading by mitotic cell rounding and non-canonical wnt signalling, *Nature Cell Biology* **21**, 169 (2018).
- [9] N. I. Petridou and C.-P. Heisenberg, Tissue rheology in embryonic organization, *The EMBO Journal* **38**, 10.15252/embj.2019102497 (2019).
- [10] R. Farhadifar, J.-C. Röper, B. Aigouy, S. Eaton, and F. Jülicher, The influence of cell mechanics, cell-cell interactions, and proliferation on epithelial packing, *Current Biology* **17**, 2095 (2007).
- [11] X. Trepaut, M. R. Wasserman, T. E. Angelini, E. Millet, D. A. Weitz, J. P. Butler, and J. J. Fredberg, Physical forces during collective cell migration, *Nature Physics* **5**, 426 (2009).
- [12] T. E. Angelini, E. Hannezo, X. Trepaut, J. J. Fredberg, and D. A. Weitz, Cell migration driven by cooperative substrate deformation patterns, *Physical Review Letters* **104**, 10.1103/physrevlett.104.168104 (2010).
- [13] K. D. Nnetu, M. Knorr, J. Käs, and M. Zink, The impact of jamming on boundaries of collectively moving weak-interacting cells, *New Journal of Physics* **14**, 115012 (2012).
- [14] E.-M. Schötz, M. Lanio, J. A. Talbot, and M. L. Manning, Glassy dynamics in three-dimensional embryonic tissues, *Journal of The Royal Society Interface* **10**, 20130726 (2013).
- [15] L. Atia, J. J. Fredberg, N. S. Gov, and A. F. Pegoraro, Are cell jamming and unjamming essential in tissue development?, *Cells & Development* **168**, 203727 (2021).
- [16] E. Lawson-Keister and M. L. Manning, Jamming and arrest of cell motion in biological tissues, *Current Opinion in Cell Biology* **72**, 146 (2021).
- [17] E. Hannezo and C.-P. Heisenberg, Rigidity transitions in development and disease, *Trends in Cell Biology* **32**, 433 (2022).
- [18] S. Garcia, E. Hannezo, J. Elgeti, J.-F. Joanny, P. Silberzan, and N. S. Gov, Physics of active jamming during collective cellular motion in a monolayer, *Proceedings of the National Academy of Sciences* **112**, 15314 (2015).
- [19] D. Bi, J. H. Lopez, J. M. Schwarz, and M. L. Manning, A density-independent rigidity transition in biological tissues, *Nature Physics* **11**, 1074 (2015).
- [20] L. Atia, D. Bi, Y. Sharma, J. A. Mitchel, B. Gweon, S. A. Koehler, S. J. DeCamp, B. Lan, J. H. Kim, R. Hirsch, A. F. Pegoraro, K. H. Lee, J. R. Starr, D. A. Weitz, A. C. Martin, J.-A. Park, J. P. Butler, and J. J. Fredberg, Geometric constraints during epithelial jamming, *Nature Physics* **14**, 613 (2018).
- [21] A. J. Liu and S. R. Nagel, Jamming is not just cool any more, *Nature* **396**, 21 (1998).
- [22] M. E. Cates, J. P. Wittmer, J.-P. Bouchaud, and P. Claudin, Jamming, force chains, and fragile matter, *Physical Review Letters* **81**, 1841 (1998).
- [23] G. Parisi and F. Zamponi, Mean-field theory of hard sphere glasses and jamming, *Reviews of Modern Physics* **82**, 789 (2010).
- [24] L. Berthier, E. Flenner, and G. Szamel, Glassy dynamics in dense systems of active particles, *The Journal of chemical physics* **150**, 200901 (2019).
- [25] L. Berthier and J. Kurchan, Non-equilibrium glass transitions in driven and active matter, *Nature Physics* **9**, 310 (2013).
- [26] É. Fodor, C. Nardini, M. E. Cates, J. Tailleur, P. Visco, and F. van Wijland, How far from equilibrium is active matter?, *Physical Review Letters* **117**, 10.1103/physrevlett.117.038103 (2016).
- [27] J.-A. Park, J. H. Kim, D. Bi, J. A. Mitchel, N. T. Qazvini, K. Tantisira, C. Y. Park, M. McGill, S.-H. Kim, B. Gweon, J. Notbohm, R. S. Jr, S. Burger, S. H. Randall, A. T. Kho, D. T. Tambe, C. Hardin, S. A. Shore, E. Israel, D. A. Weitz, D. J. Tschumperlin, E. P. Henske, S. T. Weiss, M. L. Manning, J. P. Butler, J. M. Drazen, and J. J. Fredberg, Unjamming and cell shape in the asthmatic airway epithelium, *Nature Materials* **14**, 1040 (2015).
- [28] D. Bi, X. Yang, M. C. Marchetti, and M. L. Manning, Motility-driven glass and jamming transitions in biological tissues, *Physical Review X* **6**, 10.1103/physrevx.6.021011 (2016).
- [29] N. I. Petridou, B. Corominas-Murtra, C.-P. Heisenberg, and E. Hannezo, Rigidity percolation uncovers a structural basis for embryonic tissue phase transitions, *Cell* **184**, 1914 (2021).
- [30] X. Li, A. Das, and D. Bi, Mechanical heterogeneity in tissues promotes rigidity and controls cellular invasion, *Physical Review Letters* **123**, 10.1103/physrevlett.123.058101 (2019).
- [31] T. Fuhs, F. Wetzel, A. W. Fritsch, X. Li, R. Stange, S. Pawlizak, T. R. Kießling, E. Morawetz, S. Grosser, F. Sauer, J. Lippoldt, F. Renner, S. Fribe, M. Zink, K. Bendrat, J. Braun, M. H. Oktay, J. Condeelis, S. Briest, B. Wolf, L.-C. Horn, M. Höckel, B. Aktas,

- M. C. Marchetti, M. L. Manning, A. Niendorf, D. Bi, and J. A. Käss, Rigid tumours contain soft cancer cells, *Nature Physics* **10**.1038/s41567-022-01755-0 (2022).
- [32] D. M. Sussman and M. Merkel, No unjamming transition in a voronoi model of biological tissue, *Soft Matter* **14**, 3397 (2018).
- [33] D. M. Sussman, M. Paoluzzi, M. C. Marchetti, and M. L. Manning, Anomalous glassy dynamics in simple models of dense biological tissue, *EPL (Europhysics Letters)* **121**, 36001 (2018).
- [34] M. Czajkowski, D. M. Sussman, M. C. Marchetti, and M. L. Manning, Glassy dynamics in models of confluent tissue with mitosis and apoptosis, *Soft Matter* **15**, 9133 (2019).
- [35] A. Saraswathibhatla and J. Notbohm, Tractions and stress fibers control cell shape and rearrangements in collective cell migration, *Physical Review X* **10**, 10.1103/physrevx.10.011016 (2020).
- [36] S. Kim, M. Pochitaloff, G. A. Stooke-Vaughan, and O. Campàs, Embryonic tissues as active foams, *Nature physics* **17**, 859 (2021).
- [37] A. Hopkins, M. Chiang, B. Loewe, D. Marenduzzo, and M. C. Marchetti, Local yield and compliance in active cell monolayers, *Physical Review Letters* **129**, 10.1103/physrevlett.129.148101 (2022).
- [38] S. Monfared, G. Ravichandran, J. E. Andrade, and A. Doostmohammadi, Mechanics of live cell elimination (2021).
- [39] B. Palmieri, Y. Bresler, D. Wirtz, and M. Grant, Multiple scale model for cell migration in monolayers: Elastic mismatch between cells enhances motility, *Sci. Rep.* **5**, 11745 (2015).
- [40] I. S. Aranson, ed., *Physical models of cell motility*, 1st ed., Biological and Medical Physics, Biomedical Engineering (Springer International Publishing, Basel, Switzerland, 2015).
- [41] B. A. Camley and W.-J. Rappel, Physical models of collective cell motility: from cell to tissue, *Journal of Physics D: Applied Physics* **50**, 113002 (2017).
- [42] R. Mueller, J. M. Yeomans, and A. Doostmohammadi, Emergence of active nematic behavior in monolayers of isotropic cells, *Physical Review Letters* **122**, 10.1103/physrevlett.122.048004 (2019).
- [43] A. Brugués, E. Anon, V. Conte, J. H. Veldhuis, M. Gupta, J. Colombelli, J. J. Muñoz, G. W. Brodland, B. Ladoux, and X. Trepaut, Forces driving epithelial wound healing, *Nature Physics* **10**, 683 (2014).
- [44] T. B. Saw, A. Doostmohammadi, V. Nier, L. Kocgozlu, S. Thampi, Y. Toyama, P. Marcq, C. T. Lim, J. M. Yeomans, and B. Ladoux, Topological defects in epithelia govern cell death and extrusion, *Nature* **544**, 212 (2017).
- [45] M. Abercrombie and J. E. Heaysman, Observations on the social behaviour of cells in tissue culture, *Experimental Cell Research* **6**, 293 (1954).
- [46] M. Abercrombie, Contact inhibition and malignancy, *Nature* **281**, 259 (1979).
- [47] B. Smeets, R. Alert, J. Pešek, I. Pagonabarraga, H. Ramon, and R. Vincent, Emergent structures and dynamics of cell colonies by contact inhibition of locomotion, *Proceedings of the National Academy of Sciences* **113**, 14621 (2016).
- [48] G. Peyret, R. Mueller, J. d'Alessandro, S. Begnaud, P. Marcq, R.-M. Mège, J. M. Yeomans, A. Doostmohammadi, and B. Ladoux, Sustained oscillations of epithelial cell sheets, *Biophysical Journal* **117**, 464 (2019).
- [49] T. E. Angelini, E. Hannezo, X. Trepaut, M. Marquez, J. J. Fredberg, and D. A. Weitz, Glass-like dynamics of collective cell migration, *Proceedings of the National Academy of Sciences* **108**, 4714 (2011).
- [50] J. Christoffersen, M. Mehrabadi, and S. Nemat-Nasser, A micro-mechanical description of granular material behavior, *Journal of Applied Mechanics* **48**, 339 (1984).
- [51] M. E. Fisher and A. E. Ferdinand, Interfacial, boundary, and size effects at critical points, *Physical Review Letters* **19**, 169 (1967).
- [52] M. E. Fisher and M. N. Barber, Scaling theory for finite-size effects in the critical region, *Physical Review Letters* **28**, 1516 (1972).
- [53] D. Stauffer and A. Aharony, *Introduction To Percolation Theory* (Taylor & Francis, 2018).
- [54] V. E. Debets and L. M. C. Janssen, Active glassy dynamics is unaffected by the microscopic details of self-propulsion (2022).
- [55] F. Font-Clos, S. Zapperi, and C. A. La Porta, Topography of epithelial–mesenchymal plasticity, *Proceedings of the National Academy of Sciences* **115**, 5902 (2018).
- [56] C. A. La Porta and S. Zapperi, Phase transitions in cell migration, *Nature Reviews Physics* **2**, 516 (2020).
- [57] S. Douezan, K. Guevorkian, R. Naouar, S. Dufour, D. Cuvelier, and F. Brochard-Wyart, Spreading dynamics and wetting transition of cellular aggregates, *Proceedings of the National Academy of Sciences* **108**, 7315 (2011).
- [58] C. Pérez-González, R. Alert, C. Blanch-Mercader, M. Gómez-González, T. Kolodziej, E. Bazellieres, J. Casademunt, and X. Trepaut, Active wetting of epithelial tissues, *Nature Physics* **15**, 79 (2018).
- [59] B. Ladoux, Cells guided on their journey, *Nature Physics* **5**, 377 (2009).
- [60] C. S. O'Hern, L. E. Silbert, A. J. Liu, and S. R. Nagel, Jamming at zero temperature and zero applied stress: The epitome of disorder, *Physical Review E* **68**, 10.1103/physreve.68.011306 (2003).
- [61] M. Wyart, L. E. Silbert, S. R. Nagel, and T. A. Witten, Effects of compression on the vibrational modes of marginally jammed solids, *Physical Review E* **72**, 10.1103/physreve.72.051306 (2005).
- [62] C. Toninelli, G. Biroli, and D. S. Fisher, Jamming percolation and glass transitions in lattice models, *Physical Review Letters* **96**, 10.1103/physrevlett.96.035702 (2006).
- [63] J. M. Schwarz, A. J. Liu, and L. Q. Chayes, The onset of jamming as the sudden emergence of an infinite k-core cluster, *Europhysics Letters (EPL)* **73**, 560 (2006).
- [64] M. Jeng and J. M. Schwarz, Force-balance percolation, *Physical Review E* **81**, 10.1103/physreve.81.011134 (2010).